Hindawi
Mathematical Problems in Engineering
Volume 2023, Article ID 2373118, 10 pages
https://doi.org/10.1155/2023/2373118

Research Article

Influences of Wind Deviation on the Ground Resultant Electric Field under Parallel Operation of 750-kV Ultra-High-Voltage Alternating Current and ±800-kV Extra-High-Voltage Direct Current Transmission Lines Passing through Residential Areas in a High-Altitude Area

Hui Liu,[1] Xujun Lang,[1] Ziyang Li,[1] Zhibing Sun,[1] and Shilong Huang[2]

[1]*Shandong Electric Power Engineering Consulting Institute Corp., Ltd., Jinan 250199, China*
[2]*North China Electric Power University, Baoding 071003, China*

Correspondence should be addressed to Shilong Huang; simonhuang@ncepu.edu.cn

Received 13 February 2023; Revised 26 August 2023; Accepted 25 October 2023; Published 14 November 2023

Academic Editor: Dragan Poljak

The formation mechanism of the resultant electric field is complex under parallel operation of extra-high-voltage alternating current (AC)/direct current (DC) transmission lines. However, existing methods are computationally expensive and fail to guarantee the stability and convergency of results. To solve this problem, a calculation method with nonuniform grids and varying time steps was proposed on the basis of the finite-volume and finite-element method for calculating the ground resultant electric field of parallel AC/DC transmission lines. The selection of the initial value of space charges and the setting of the surface charge density of conductors were also improved, which greatly enhanced the computational stability and efficiency. Then, the improved method was adopted to calculate the ground resultant electric field under parallel operation of a 750-kV AC transmission line and a ±800-kV DC transmission line when considering and not considering wind deviation. Results show that, when ignoring wind deviation, the normalized values of the ground resultant electric field within 6 m from the side-phase conductor of the AC line are always less than 1 under conditions of the minimum clearances to earth of the AC and DC lines passing through a residential area stipulated in the national standards, which meets codified requirements. When considering wind deviation, instead of an increase, the calculated ground resultant electric field of parallel AC/DC lines is significantly reduced, and the weighted value is much less than the limiting value.

1. Introduction

With the rapid development of the power sector in China, the transmission line corridors are increasingly scarce, so the parallel operations of alternating current (AC) and direct current (DC) transmission lines in the same corridor have become more common [1, 2]. If AC and DC lines are erected adjacent to each other, processes including ion production, ionic drift, and ionic recombination accompanying the corona discharge of DC lines will be influenced, thus forming a resultant electric field [3, 4]. To design AC/DC lines in a same corridor or on the same tower and then control the ground ion flow field, calculation methods for the resultant electric field of parallel AC/DC lines need to be warranted.

Chartier et al. [5] studied the ground electromagnetic environment after changing one circuit of an AC double-circuit transmission line on a same tower into a ±500-kV DC line and proposed an empirical equation for calculating the resultant electric field. When calculating the resultant electric field, they believed that the DC and AC components of the resultant electric field can be calculated separately and then summed. Maruvada and Drogi [6] stated that the presence of an AC line exerts slight influences on the drift trajectory of ions produced by the DC line. Therefore, they proposed

to adopt the flux-line method to calculate the DC component of the resultant electric field, then calculated the AC component independently, and finally obtained the resultant electric field by summation of the two components. Abdel-Salam et al. [7] used the charge simulation method to calculate the ground electric field arising from parallel AC/DC lines, however, the calculation process does not consider distortion effects of ions on the electric field, so the method is only applicable to cases with low-voltage of DC lines. Based on the previous experimental results of the Electric Power Research Institute (EPRI), scholars in Ohio State University conducted experiments on the corona field of parallel AC/DC lines by using a reduced-scale model [8]. Thereafter, Zhao et al. [9] developed a method that can calculate the DC corona loss and corona current on the DC and AC conductors, and the ground electric field intensity and ion current density based on the previous experimental results.

Li et al. [10] working in Tsinghua University, took the lead to use the time-domain analysis method to study the ion flow field and resultant electric field of AC/DC lines sharing the same corridor and proposed the time-domain upwind finite-element method. Yang et al. [11] working in Beijing University of Aeronautics and Astronautics, adopted the flux-line method to explore the distribution of the ground electric field intensity under the condition that AC/DC lines share the same corridor. Based on a reduced-scale experimental model, Zhang et al. [12] working in Tsinghua University investigated the ground ion flow and resultant electric field of AC/DC lines. In addition, staff at the China Electric Power Research Institute also conducted many studies focusing on the electromagnetic environment of hybrid AC/DC transmission lines and made great efforts. These include research on calculation methods for the AC/DC resultant electric field and the minimum approach distance of transmission lines in the same corridor and their experimental verification [3]. Huang et al. [13] investigated the corona onset characteristics of bundle conductors at high-altitude areas. Choopum and Techaumnat [14] investigated the effects of wind and shielding conductor on the ion flow fields of HVDC transmission lines. Li and Zhao [15] calculated the ion flow field of monopolar transmission line in corona cage including the effect of wind.

The above analysis indicates that scholars widely use the time-domain finite-element method to carry out AC/DC coupling calculation of ion flows considering the effect of ion flow fields in AC/DC electric fields at present. However, existing methods are computationally expensive and cannot guarantee the stability and convergency of the calculation results. Besides, there is also little research on the influences of wind deviation on the resultant electric field of parallel AC/DC lines at high-altitude areas. Therefore, a method of calculation with nonuniform grids and varying time steps was proposed based on the finite-volume and finite-element method for calculating the ground resultant electric field of parallel AC/DC lines. Moreover, the selection of the initial value of space charges and the setting of the surface charge density of conductors were improved. The improved method was adopted to calculate ground resultant electric fields under the parallel operation of a 750-kV AC line and a $\pm$800-kV DC line when considering, and ignoring wind deviation.

2. The Finite-Volume and Finite-Element Method for Calculating the Resultant Electric Field

2.1. Calculation Procedures. The calculation procedures for the resultant electric field of parallel AC and DC lines are illustrated in Figure 1. The resultant electric field and space charge density were calculated at any moment and boundary conditions for the surface charge density of conductors were updated according to the electrical potential of the AC conductors at that moment. The calculation lasted for several AC cycles until meeting the termination criterion. The resultant electric field and the distribution of the space charge density at each moment in the last AC cycle were recorded in the results.

2.2. Time-Dependent Upwind Difference Discretization. If there is an AC electric field in a space, the electric field and the charge density at each point in the space both change with time. Compared with the governing equations of the DC ion flow field, the governing equations of AC/DC hybrid ion flow field are changed after adding a time term as follows:

The Poisson's equations are

$$\nabla^2 \Phi(t) = -(\rho^+(t) - \rho^-(t))/\varepsilon_0, \tag{1}$$

$$\Phi(t) = \phi_{\mathrm{DC}}(t) + \phi_{\mathrm{AC}}(t) + \phi(t), \tag{2}$$

where $\Phi(t)$ represents the space electrical potential, which is composed of three parts: ϕ_{DC} is the nominal DC potential that does not change with time; $\phi_{\mathrm{AC}}(t)$ is the nominal AC potential; and $\phi(t)$ is the electrical potential produced by the space charges. $\rho^+(t)$ and $\rho^-(t)$ denote the positive and negative charge densities, respectively.

The ion flow equations are

$$\boldsymbol{j}^+(t) = \rho^+(t)(-k^+ \nabla \Phi(t) + \boldsymbol{W}(t)), \tag{3}$$

$$\boldsymbol{j}^-(t) = \rho^-(t)(-k^- \nabla \Phi(t) - \boldsymbol{W}(t)), \tag{4}$$

where $\boldsymbol{j}^+(t)$ and $\boldsymbol{j}^-(t)$ separately represent the positive and negative ion current densities; k^+ and k^- separately denote the positive and negative ion mobility; $\boldsymbol{W}(t)$ is the wind speed.

The continuity equations for the electric current are

$$\frac{\partial \rho^+(t)}{\partial t} = -\nabla \cdot \boldsymbol{j}^+(t) - R\rho^+(t)\rho^-(t)/e, \tag{5}$$

$$\frac{\partial \rho^-(t)}{\partial t} = -\nabla \cdot \boldsymbol{j}^-(t) - R\rho^-(t)\rho^+(t)/e, \tag{6}$$

where R indicates the recombination coefficient of positive and negative ions; e denotes the electron charge.

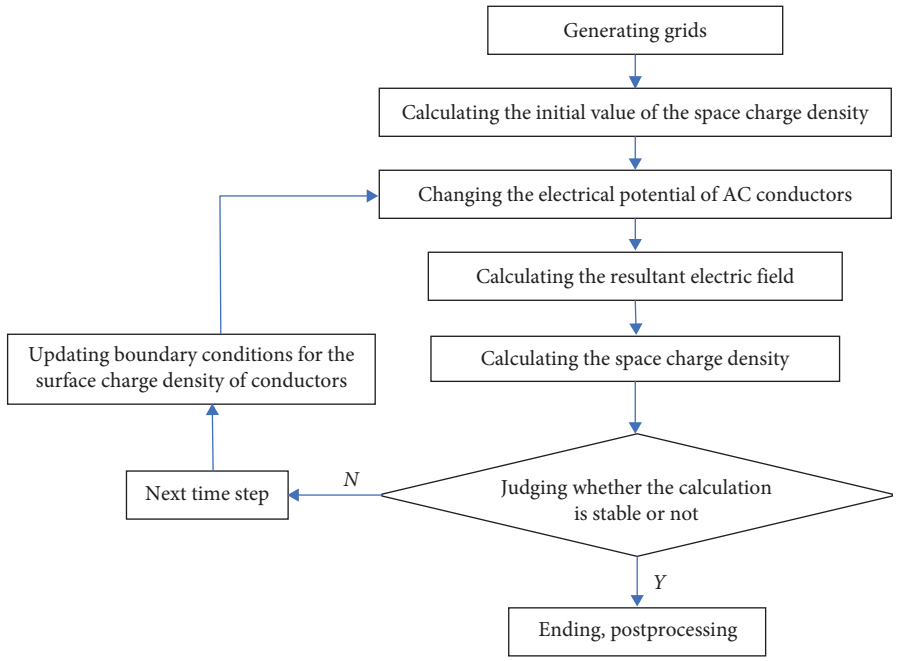

Figure 1: Calculation procedures for the resultant electric field of parallel AC and DC lines.

$\phi_{DC}(t), \phi_{AC}(t)$, and $\phi(t)$ in Equation (2) are separately calculated; $\phi_{\mathrm{DC}}(t)$ and $\phi_{\mathrm{AC}}(t)$ are computed using charge simulation method while $\phi(t)$ is calculated using the finite-element method.

The concept of upwind difference is introduced to calculation of the space charge density. Combining Equations (1)–(6) gives

$$\frac{\partial \rho^+(t)}{\partial t} = -\boldsymbol{V}^+(t)\operatorname{grad}\rho^+(t) - \frac{k^+}{\varepsilon_0}(\rho^+(t))^2 + \left(\frac{k^+}{\varepsilon_0} - \frac{R}{e}\right)\rho^+(t)\rho^-(t), \tag{7}$$

$$\frac{\partial \rho^-(t)}{\partial t} = -\boldsymbol{V}^-(t)\operatorname{grad}\rho^-(t) - \frac{k^-}{\varepsilon_0}(\rho^-(t))^2 + \left(\frac{k^-}{\varepsilon_0} - \frac{R}{e}\right)\rho^+(t)\rho^-(t), \tag{8}$$

where $\boldsymbol{V}^+(t) = -k^+\operatorname{grad}\Phi(t) + \boldsymbol{W}(t)$ and $\boldsymbol{V}^-(t) = k^-\operatorname{grad}\Phi(t) + \boldsymbol{W}(t)$.

The space is divided using triangular grids. Node i and its surrounding elements are shown in Figure 2. On node i, there are

$$\frac{\partial \rho_i^+(t)}{\partial t} = -\boldsymbol{V}_i^+(t)\operatorname{grad}\rho_i^+(t) - \frac{k^+}{\varepsilon_0}(\rho_i^+(t))^2 + \left(\frac{k^+}{\varepsilon_0} - \frac{R}{e}\right)\rho_i^+(t)\rho_i^-(t), \tag{9}$$

$$\frac{\partial \rho_i^-(t)}{\partial t} = -\boldsymbol{V}_i^-(t)\operatorname{grad}\rho_i^-(t) - \frac{k^-}{\varepsilon_0}(\rho_i^-(t))^2 + \left(\frac{k^-}{\varepsilon_0} - \frac{R}{e}\right)\rho_i^+(t)\rho_i^-(t), \tag{10}$$

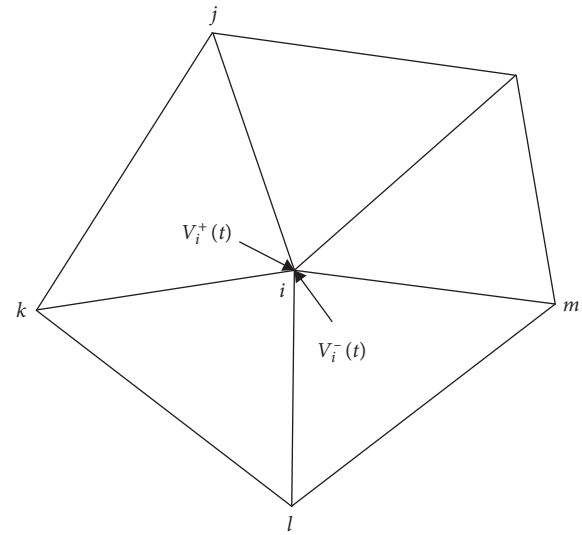

Figure 2: Upwind elements of nodes.

where $\boldsymbol{V}_i^+(t) = -k^+\operatorname{grad}\Phi_i(t) + \boldsymbol{W}(t)$ and $\boldsymbol{V}_i^-(t) = k^-\operatorname{grad}\Phi_i(t) + \boldsymbol{W}(t)$.

$\boldsymbol{V}_i^+(t)$ and $\boldsymbol{V}_i^-(t)$ can be regarded as the motion speeds of positive and negative charges at point i. Due to the high amplitude of the space electric field, charges mainly migrate, and the positive and negative charge densities at point i are considered to be related only to elements (termed as upwind elements) opposite to the motion directions of positive and negative charges. That is, the positive charge density at point i in Figure 2 is only related to Δijk, while the negative charge density is only related to Δilm. First-order discretization on Equations (9) and (10) in upwind elements gives

$$\frac{\rho_i^+(t_{n+1}) - \rho_i^+(t_n)}{\Delta t} = -\left(-k^+ \operatorname{grad} \Phi_{\Delta ijk}(t_n) + \boldsymbol{W}(t_n)\right) \operatorname{grad} \rho_{\Delta ijk}^+(t_n) - \frac{k^+}{\varepsilon_0}(\rho_i^+(t_n))^2 + \left(\frac{k^+}{\varepsilon_0} - \frac{R}{e}\right)\rho_i^+(t_n)\rho_i^-(t_n), \quad (11)$$

$$\frac{\rho_i^-(t_{n+1}) - \rho_i^-(t_n)}{\Delta t} = -(k^- \operatorname{grad} \Phi_{\Delta ilm}(t_n) + \boldsymbol{W}(t_n)) \operatorname{grad} \rho_{\Delta ilm}^-(t_n) - \frac{k^-}{\varepsilon_0}(\rho_i^-(t_n))^2 + \left(\frac{k^-}{\varepsilon_0} - \frac{R}{e}\right)\rho_i^-(t_n)\rho_i^+(t_n), \quad (12)$$

where $\Phi_{\Delta ijk}(t_n)$ and $\Phi_{\Delta ilm}(t_n)$ separately denote electrical potentials in elements Δijk and Δilm at time t_n; $\operatorname{grad} \rho_{\Delta ijk}^+(t_n)$ is the positive charge density gradient in element Δijk at time t_n; $\operatorname{grad} \rho_{\Delta ilm}^-(t_n)$ is the negative charge density gradient in element Δilm at time t_n.

2.3. Simplification of the Calculation Method When AC and DC Transmission Lines Are Erected in Parallel. When AC and DC lines are erected in parallel, the DC line will induce a DC electric field in the area of the AC line. However, the maximum value of the AC electric field in the area is significantly larger than the induced DC electric field because space charges of the AC line are concentrated near the conductor. Therefore, the motion of the space charges produced by corona of the AC line exerts little influence on the induced DC electric field, while on the AC conductor surface, the maximum value of the AC electric field is much greater than the induced DC electric field, so the induced DC electric field also exerts slight influences on corona of the AC conductor. Considering this, influences of the DC line on the corona field of the AC line are ignored. There are many space charges below the DC line, so the AC electric field induced by the AC line in the corridor of the DC line affects the motion of these space charges. Therefore, to reduce the computational burden, the corona effect of the AC line was ignored while only the ion flow field in the corridor of the DC line was considered. That is, mesh generation was only performed near the DC line. By using the calculation method for the corona loss of AC lines based on the charge simulation method, the AC electric field generated by the AC line in the computational area below the DC line can be calculated considering the strengthening effect of corona on the AC electric field. The value of the AC electric field in the computation area below the DC line is recalculated at each moment, and it is superimposed on the DC resultant electric field to affect motion behaviors of the space charges below the DC line. The rationality of the above hypothesis is proved in [5].

2.4. Calculation Method with Nonuniform Grids and Varying Time Steps. For the explicit difference calculation method given by Equations (11) and (12), the selection of time steps should guarantee that the transmission speed of charge density information between nodes is lower than the charge migration speed, otherwise, the results may diverge with time.

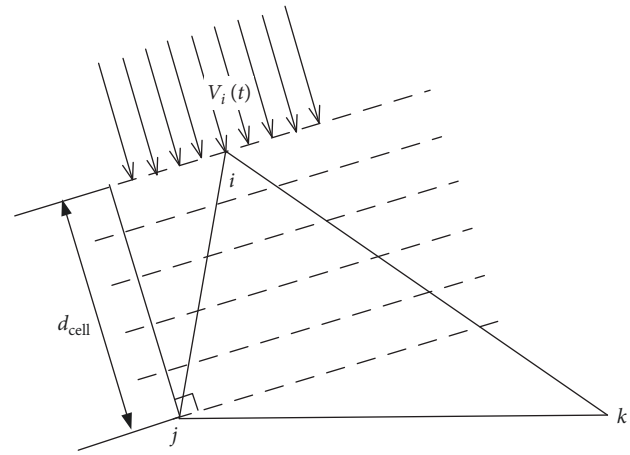

FIGURE 3: Limitation on the time step.

In the first-order triangular element Δijk shown in Figure 3, the space charge density at node i is given at time t and the motion speed of space charges is $\boldsymbol{V}_i(t) = -k \operatorname{grad} \Phi_i(t) + \boldsymbol{W}(t)$. The direction of motion is shown in the figure. Node j is a node downstream of node i, and d_{cell} represents the projection of the distance between i and j in the V_i-direction. To ensure that the transmission speed of the charge density information between nodes i and j is lower than the charge migration speed, then

$$dt \le \frac{d_{\text{cell}}}{|\boldsymbol{V}_i|}. \quad (13)$$

Equation (13) indicates that for each grid to be calculated, there is limitation on the maximum time step. Too small a time step will increase the computational burden, so the time step in the calculation must be chosen with care.

To improve the calculation speed, a calculation method with nonuniform elements and varying time steps was proposed. That is, some elements (but not all) are determined to participate in calculation according to the mesh size and the charge migration speed at each moment, so as to reduce the computational burden. To be specific, the minimum value dt_0 of the maximum time step of all grid elements is calculated at the beginning to serve as the overall time step of calculation. If the maximum time step dt_i of element e_i at each moment is an integral multiple of dt_0, the element e_i takes part in the calculation; otherwise, e_i does not take part in calculation. In practical operation, the set of mesh elements $\{e_i\}$ meeting the following equation is sought:

$$N \times dt_0 \le dt_i < (N+1) \times dt_0, \quad (14)$$

where N is an integer.

For each grid node not on the boundary, its upwind elements are calculated. For the node set $\{n_i\}$, the upwind elements of which are in the set $\{e_i\}$, their charge density at the next moment is calculated using Equations (11) and (12). In this way, the time step is spatially nonuniform; the

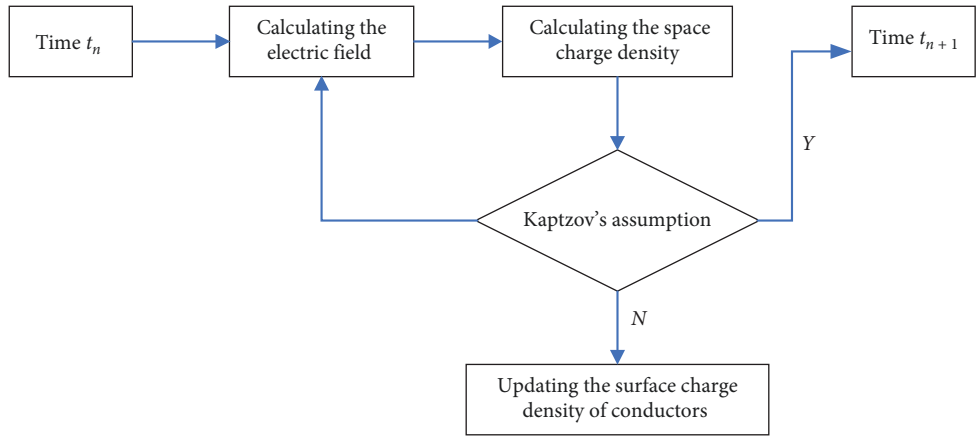

FIGURE 4: The iterative process used to calculate the surface charge density of conductors.

number of mesh elements taking part in the calculation changes at each time step in terms of the number of calculation steps.

2.5. Selection of the Initial Value of Space Charges. The selection of the initial value of space charges exerts significant influences on the computational stability and convergence. When AC and DC electric fields are present simultaneously, the computation will not reach stability until calculation after 10 of AC cycles from the initial value 0. The above analysis implies that space charges mainly move from the high to low electrical potential under action of the DC electric field in the AC/DC resultant electric field; because the AC electric field can be regarded as a disturbance superimposed on the DC electric field, the calculation results for distribution of the DC steady-state space charge density without the AC electric field can be used as the initial value of the AC/DC resultant electric field, so that the calculation can converge more rapidly.

2.6. Setting of the Surface Charge Density of Conductors. The surface charge density of conductors is a boundary condition for calculating the distribution of the space charge density. At the beginning of calculation, the DC steady-state surface charge density of conductors without AC electric field is used as the initial value. Under these conditions, the electric field on conductor surfaces satisfies Kaptzov's assumption. Afterward, the surface charge density of conductors changes correspondingly at each moment with variation of the AC electric field and must be obtained before calculating the distribution of the space charge density. If the electric field on the conductor surface in the AC/DC resultant electric field still meets Kaptzov's assumption, then the iterative method shown in Figure 4 is adopted at each moment to determine the surface charge density of the conductors.

Based on the assumption that the AC electric field is a disturbance to the DC electric field, the ratio of the surface charge density of conductors in the AC/DC resultant electric field to that in the DC steady-state ion flow field is regarded same as the ratio of the difference between nominal electric field and corona inception field intensity of the two, that is,

$$\frac{\rho_t}{\rho_0} = \frac{E_{t,n} - E_c}{E_{0,n} - E_c}. \tag{15}$$

Hence, the surface charge density of conductors at each moment in the AC/DC resultant electric field is written as follows:

$$\rho_t = \frac{E_{t,n} - E_c}{E_{0,n} - E_c} \cdot \rho_0. \tag{16}$$

Compared with the case of using the iterative method, the above equation incurs a slight loss in computational accuracy while it significantly improves the computation speed.

2.7. Termination Criterion. Whether the calculation results meet the accuracy requirement or not is judged when the current time t is an integral multiple of the AC cycle (0.02 s). The difference between the initial and final space charge densities in the final AC cycle is taken as the termination criterion, that is,

$$\frac{\sum_{N_{\text{node}}} \left(\left| \rho^{+}_{(N+1)\times ts,i} - \rho^{+}_{N\times ts,i} \right| + \left| \rho^{-}_{(N+1)\times ts,i} - \rho^{-}_{N\times ts,i} \right| \right)}{N_{\text{node}}} \le \varepsilon, \tag{17}$$

where $i = 1, \cdots, N_{\text{node}}$, and N_{node} represents the total number of nodes; N is an integer; ts and ε are the AC cycle (0.02 s) and error tolerance, respectively. $\rho^{+}_{N\times ts,\,i}$ and $\rho^{-}_{N\times ts,\,i}$ separately denote the positive and negative charge densities at the ith node at time $N \times S\,ts$. The relative error of the two iterations is less than 0.01%.

The calculation is stopped if the termination criterion is satisfied. The space charge densities and resultant electric fields in the final two AC cycles are stored. If the termination criterion is not met, the calculation enters the next AC cycle. The algorithm is realized by MATLAB programing, the operating hardware environment is CPU-12th Gen Intel (R), Core (TM)-i9-12900KF, 3.20 GHz, 128 Gbit memory.

Table 1: Parameter setting.

	Conductor model	Ground wire model	Roughness coefficient
AC	6 × LGJ-400/50	GJ-100/OPGW-120	0.8
DC	6 × JL/G3A-1000/45	JLHA1/LB1-180/30	0.46

3. Calculation and Analysis of the Ground Resultant Electric Field of Parallel AC/DC Lines Passing through a Residential Area

3.1. Limit of the Electric Field of AC/DC Lines. If transmission lines are close to the residential buildings, the control limit of the power frequency electric field of an individual AC transmission line is the maximum undistorted field intensity 1 m above the ground-level at the buildings, which does not exceed 4 kV/m; for an individual DC transmission line, the control limit of the ground resultant electric field is at the position of the buildings, which does not exceed 15 kV/m when calculating under conditions involving wet conductors.

At present, there are still no national and overseas standards for the control limit of the resultant electric field of AC/DC lines that are erected in a same corridor. Based on the previous control limits of electric fields of AC and DC lines, the weighting method was employed to determine the control limit of the AC/DC resultant electric field. The weighting method is described as follows:

$$\frac{\text{Electric fields of AC lines}}{\text{control limits of AC lines}} + \frac{\text{Electric fields of DC lines}}{\text{control limits of DC lines}} \leq 1. \tag{18}$$

For the control of the electric field of AC/DC lines in the same corridor, the control limits of the AC and DC electric fields at the position of residential buildings are separately 4 and 15 kV/m if such AC/DC lines are close to the residential buildings.

3.2. Calculation of the Ground Resultant Electric Field of Parallel AC/DC Lines When Not Considering Wind Deviation. It is stipulated in the national standards that if conductors pass through a residential area, the minimum clearances to earth of ±800-kV DC lines and 750-kV AC lines should be 21 and 19.5 m, respectively. Therefore, the clearances to earth of the DC conductor and the AC conductor were separately set at 21 and 19.5 m. Other parameters of the AC/DC lines in the high-altitude area are set as in Table 1. The model with the grid is shown in Figure 5.

Figure 6 displays distribution of the instantaneous maximum value of the ground resultant electric field of the AC/DC lines when the center-to-center spacing between AC and DC lines is 90 m. Figure 7 shows the distribution curves of normalized values of the electric field calculated using the weighting method of AC and DC electric fields when the center-to-center spacing between AC and DC lines is 90 m. The normalized values are all less than 1 when the center-to-center spacing is 90 m, which meets the requirement for the limit of the ground electric field. In addition,

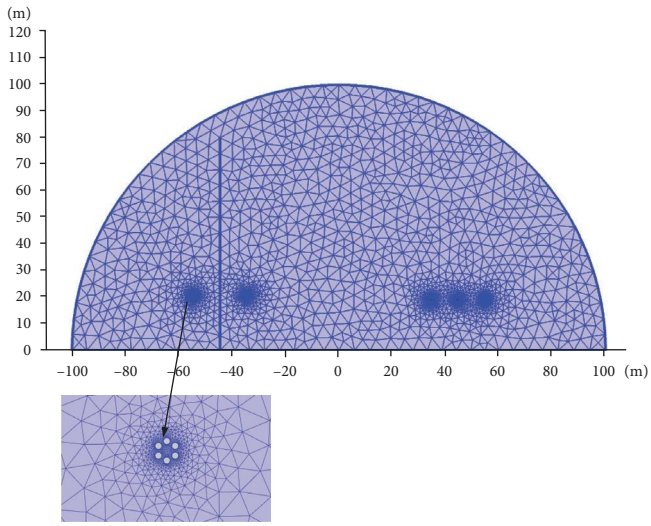

Figure 5: The model with the grid of the parallel AC/DC lines.

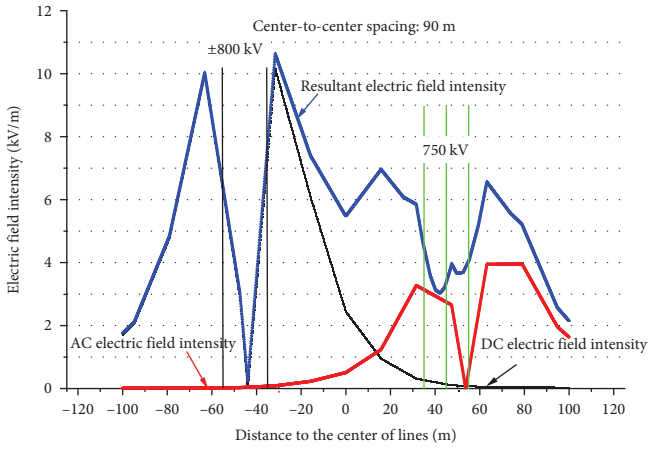

Figure 6: Instantaneous maximum value of the ground resultants electric field of the parallel AC/DC lines.

according to the national standards, no residential buildings are allowed to be built within a range of 6 m outside the projection of the side-phase conductor of 750-kV lines. Besides, it is necessary that the distorted electric field at the height of 1.5 m above ground at the location of the buildings should not exceed 4 kV/m. It is calculated that the normalized value is less than 1 at a location 6 m from the side-phase conductor of the AC line, which meets the codified requirement.

3.3. Calculation of the Ground Resultant Electric Field of Parallel AC/DC Lines When Considering Wind Deviation. Factors including wind deviation of insulator strings and

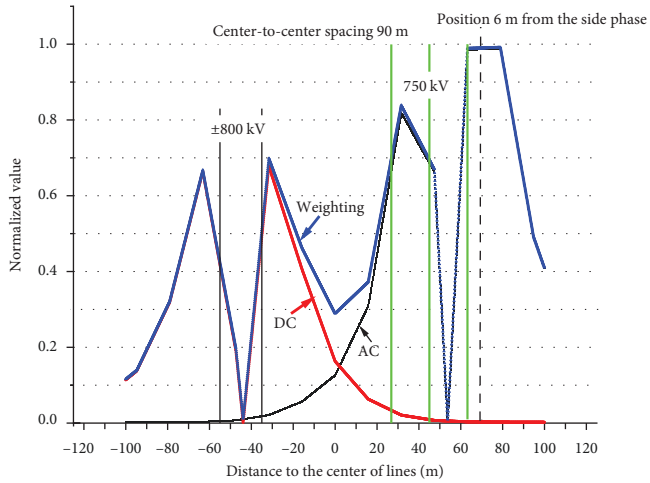

Figure 7: Normalized value of the ground electric field of the parallel AC/DC lines.

Table 2: Wind deviation parameters of insulator strings.

Conductor	DC (± 800 kV)		AC (750 kV)		
	−	+	Side Phase A	Middle Phase B	Side Phase C
Type of insulator string	V-shaped insulator string	V-shaped insulator string	I-shaped insulator string	V-shaped insulator string	I-shaped insulator string
String length/m	11.8	11.8	8	8.8	8
Included angle	85°	85°	/	90°	/
Angle of wind deviation	15°	15°	40°	15°	40°
Horizontal offset ΔX/m	1.98	1.98	5.14	1.37	5.14
Vertical offset ΔY/m	2.36	2.36	2.86	1.85	2.86

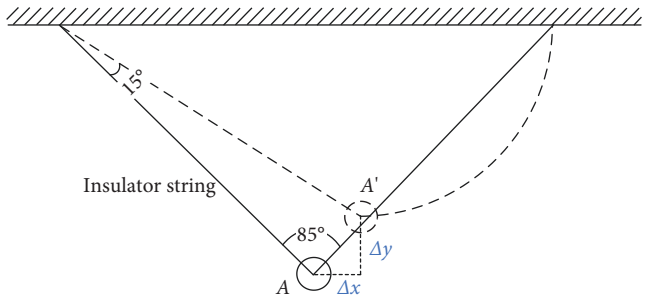

Figure 8: Wind deviation of a V-shaped insulator string on the ± 800-kV DC line.

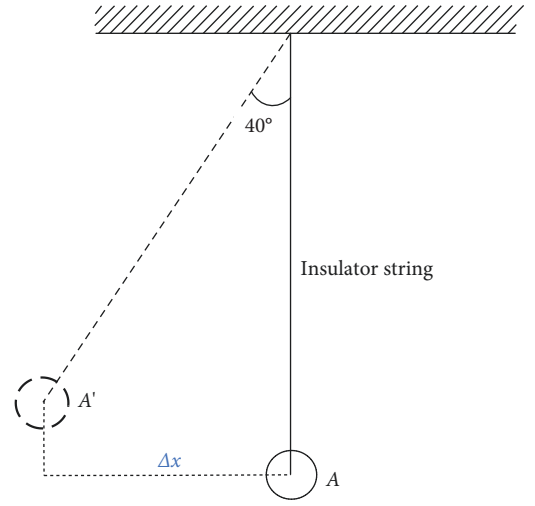

Figure 9: Wind deviation of an I-shaped insulator string on the 750-kV AC line.

conductor swinging are considered when calculating influences of wind deviation on the ground resultant electric field of parallel AC and DC lines. The magnitude of wind deviation of insulator strings is related to the span of lines, types of insulator strings, and wind speed, which have been widely studied by many scholars. The influences of wind deviation on the ground resultant electric field are mainly calculated, so the calculation of wind deviation is not highlighted while only the magnitude of wind deviation was provided, as listed in Table 2.

Figures 8–10 show the wind deviation of insulator strings, in which V-shaped insulator strings are adopted to the ±800-kV DC line and the 750-kV AC line. V-shaped insulator strings can effectively limit the swinging, so the wind-induced deviation is small. The I-shaped insulator string is used for the side phases of the 750-kV AC line, which shows large wind deviation due to poor stability.

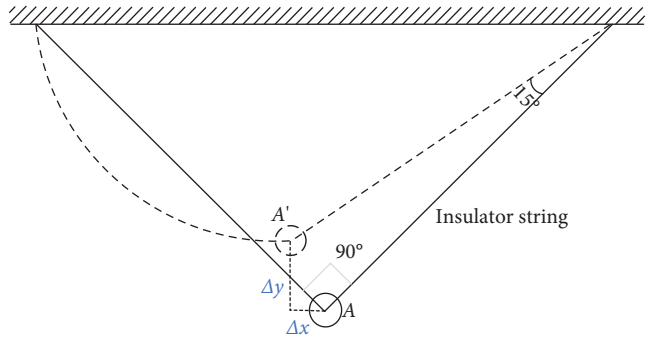

Figure 10: Wind deviation of a V-shaped insulator string on the 750-kV AC line.

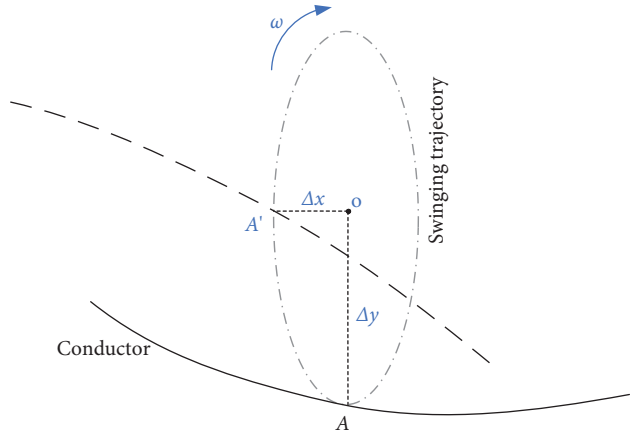

Figure 11: A swinging conductor.

Table 3: Horizontal and vertical offsets of the conductors when considering the wind deviation

Classification	Horizontal and vertical offsets	±800 kV	750 kV	
		V-shaped insulator string	V-shaped insulator string	I-shaped insulator string
Wind deviation of insulator strings	D*X*/m	1.98	1.37	5.14
	D*Y*/m	2.36	1.85	2.86
Conductor swinging	D*X*/m	2	2	2
	D*Y*/m	5	5	5
Total offset	D*X*/m	3.98	3.37	7.14
	D*Y*/m	7.36	6.85	7.86

Generally, conductor swinging is likely to happen to ice-covered eccentric bundle conductors, which are commonly erected in flat and open areas or areas across water. The included angle between wind and lines exceeds 45° and the wind speed remains stable between 5 and 20 m/s. The swinging trajectory is commonly an ellipse with the vertical offset as the long axis, often accompanied by synchronous alternating torsion of conductors around the phase axis. The amplitude is proportional to the span and sag, the swinging height generally does not exceed the connection between wave nodes, and the bottom of the arc is not lower than the sag of the conductor.

A relatively serious case of conductor swinging is taken, with the amplitude and horizontal offset set to be 10 and 4 m, respectively. Therefore, the long and short axes of the elliptical motion trajectory are separately 10 and 4 m. When the conductor swings to the short axis, the horizontal offset is the largest, namely, $\Delta X = 2$ m and $DY = 5$ m, as illustrated in Figure 11.

Under parallel transmission of the AC/DC lines, there is a case with the minimum approach distance between the AC and DC conductors considering the asynchronous swinging of conductors. That is, the wind deviation of insulator strings and the conductor swinging can be considered at the same time. When considering wind deviation, the horizontal and vertical offsets of the conductors are as listed in Table 3.

Wind deviation of conductors that pass through a residential area was calculated. Wind deviation of conductors is

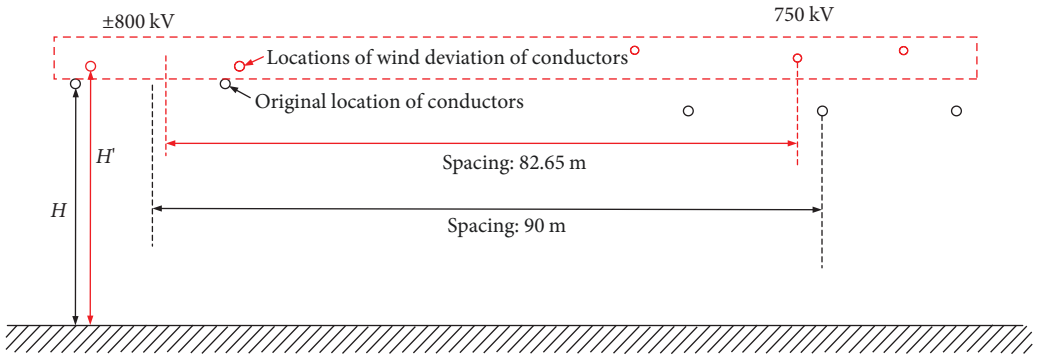

Figure 12: Wind deviation of conductors on the parallel AC/DC lines (residential area).

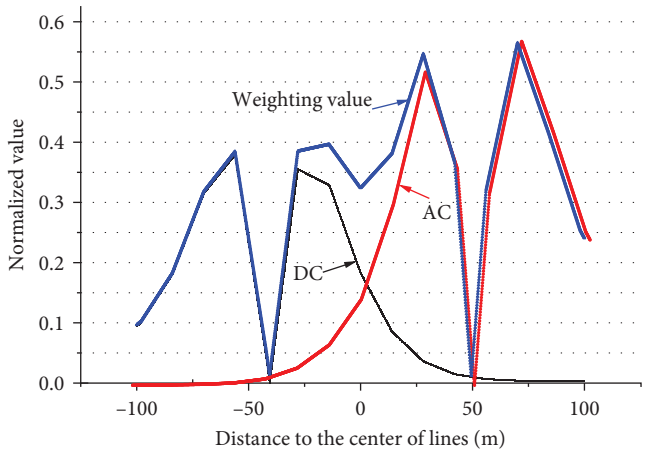

Figure 13: Distribution of normalized values of the ground electric field when considering wind deviation.

illustrated in Figure 12 and the calculated, normalized values of the ground electric field are shown in Figure 13.

As shown in Figure 13, the maximum weighted value of the ground resultant electric field is about 0.55, which is much less than 1. This is because although the wind deviation narrows the spacing between conductors, it also increases the heights of conductors. Therefore, instead of increases, the ground electric field is found to be largely decreased, so influences of wind deviation can be ignored when calculating the minimum spacing between the parallel AC/DC lines.

4. Conclusions

(1) Based on the finite-volume and finite-element method of calculating the ground resultant electric field of parallel AC/DC lines, the calculation method with nonuniform grids and varying time steps was proposed. The selection of the initial value of space charges and the setting of the surface charge density of conductors were improved, which substantially enhanced the computational stability and efficiency;

(2) The improved method was used to calculate the ground resultant electric field during parallel operation of the 750-kV AC line and the ±800-kV DC line in the high-altitude area without considering wind deviation. Calculations show that the normalized values of the ground resultant electric field and that within 6 m from the side-phase conductor of the AC line are both lower than 1 under conditions of the minimum clearances to earth of the AC and DC lines in the residential area stipulated in national standards, which meets design requirements;

(3) Under wind deviation of insulator strings and conductor swinging, instead of increases, a great reduction of the calculated ground resultant electric field of parallel AC/DC lines is found, and the weighted values are far lower than the limiting value.

(4) For the design of hybrid overhead lines, the influence of wind deviation does not need to be considered from the perspective of resultant electric field, but for insulation design such as air gap, the influence of wind deviation still needs to be considered.

Data Availability

The data used to support the findings of this study are included within the article.

Conflicts of Interest

The authors declare that they have no conflicts of interest.

Acknowledgments

This work is supported by the Natural Science Foundation of China (52007063).

References

[1] B. Tang, H. Jiang, R. Sun, R. Liu, and Z. Wu, "Calculation of power frequency electric field for AC parallel transmission lines in the same corridor based on MOM," *High Voltage Apparatus*, vol. 54, no. 12, pp. 104–109, 2018.

[2] S. Shuai, L. Tiebing, and C. Xiang, "The characteristics of hybrid electric field under the DC wire parallel with the AC wire," *Transactions of China Electrotechnical Society*, vol. 32, no. 8, pp. 138–143, 2017.

[3] G.-F. Wu, C.-F. Yuan, J.-Y. Lu, Y. Ju, L.-X. ZHao, and Y. Yang, *Calculation on Electromagnetic Environment of UHVDC and EHVAC Transmission Lines Erected in a Common Corridor*, vol. 34, pp. 14–19, Power System Technology, 2010.

[4] Y. Zhao and W. Zhang, *Research on Hybrid Electric Field Caused by HVAC and HVDC Transmission Lines Erected on the Same Tower*, vol. 38, pp. 120–125, Power System Technology, 2014.

[5] V. L. Chartier, S. H. Sarkinen, R. D. Stearns, and A. L. Burns, "Investigation of corona and field effects of AC/DC hybrid transmission lines," *IEEE Transactions on Power Apparatus and Systems*, vol. 1PAS-100, pp. 72–80, 1981.

[6] P. S. Maruvada and S. Drogi, "Field and ion interactions of hybrid AC/DC transmission lines," *IEEE Transactions on Power Delivery*, vol. 3, no. 3, pp. 1165–1172, 1988.

[7] M. Abdel-Salam, M. T. El-Mohandes, and H. El-Kishky, "Electric field around parallel DC and multi-phase AC transmission lines," *IEEE Transactions on Electrical Insulation*, vol. 25, no. 6, pp. 1145–1152, 1990.

[8] D. G. Kasten, S. A. Sebo, T. Zhao, L. E. Zaffanella, and B. A. Clairmont, "Corona tests on reduced-scale two-conductor hybrid lines," in *Proceedings of IEEE Conference on Electrical Insulation and Dielectric Phenomena*, pp. 624–629, IEEE, 1993, 1993.

[9] T. Zhao, S. A. Sebo, and D. G. Kasten, "Calculation of single phase AC and monopolar DC hybrid corona effects," *IEEE Transactions on Power Delivery*, vol. 11, no. 3, pp. 1454–1463, 1996.

[10] W. Li, J. He, B. Zhang, R. Zeng, X. Li, and Q. Wang, "Calculation of the ion flow field of AC–DC hybrid transmission lines," *IET Generation, Transmission & Distribution*, vol. 3, no. 10, pp. 911–918, 2009.

[11] Y. Yang, J. Lu, and Y. Lei, "A calculation method for the hybrid electric field under UHVAC and UHVDC transmission lines in the same corridor," *IEEE Transactions on Power Delivery*, vol. 25, no. 2, pp. 1146–1153, 2010.

[12] B. Zhang, W. Li, J. He, and R. Zeng, "Study on the field effects under reduced-scale DC/AC hybrid transmission lines," *IET Generation, Transmission & Distribution*, vol. 7, no. 7, pp. 717–723, 2013.

[13] S. Huang, Y. Liu, S. Chen, G. Zhou, and W. Zhuang, "Corona onset characteristics of bundle conductors in UHV AC power lines at 2200 m altitude," *Energies*, vol. 11, no. 5, Article ID 1047, 2018.

[14] C. Choopum and B. Techaumnat, "Numerical Investigation on the effects of wind and shielding conductor on the ion flow fields of HVDC transmission lines," *Energies*, vol. 16, no. 1, Article ID 198, 2023.

[15] Z. Li and X. Zhao, "Calculation of ion flow field of monopolar transmission line in corona cage including the effect of wind," *Energies*, vol. 12, no. 20, Article ID 3924, 2019.